Optics and Laser Technology 96 (2017) 50–57

Contents lists available at ScienceDirect

Optics and Laser Technology

journal homepage: www.elsevier.com/locate/jolt

Full length article

Robustness of an artificially tailored fisheye imaging system with a curvilinear image surface

Gil Ju Lee [a], Won Il Nam [b], Young Min Song [a,*]

[a] School of Electrical Engineering and Computer Science, Gwangju Institute of Science and Technology, 123 Cheomdangwagi-ro, Buk-gu, Gwangju 61005, Republic of Korea
[b] Department of Electronics Engineering, Pusan National University, 2 Busandaehak-ro 63-beon-gil, Geumjeong-gu, Busan 609-735, Republic of Korea

ARTICLE INFO

Article history:
Received 31 January 2017
Accepted 28 April 2017
Available online 18 May 2017

Keywords:
Lens system design
Photodetector
Optical engineering
Biomimetic imaging devices
Flexible optoelectronics

ABSTRACT

Curved image sensors inspired by animal and insect eyes have provided a new development direction in next-generation digital cameras. It is known that natural fish eyes afford an extremely wide field of view (FOV) imaging due to the geometrical properties of the spherical lens and hemispherical retina. However, its inherent drawbacks, such as the low off-axis illumination and the fabrication difficulty of a 'dome-like' hemispherical imager, limit the development of bio-inspired wide FOV cameras. Here, a new type of fisheye imaging system is introduced that has simple lens configurations with a curvilinear image surface, while maintaining high off-axis illumination and a wide FOV. Moreover, through comparisons with commercial conventional fisheye designs, it is determined that the volume and required number of optical elements of the proposed design is practical while capturing the fundamental optical performances. Detailed design guidelines for tailoring the proposed optic system are also discussed.

1. Introduction

In lens design, it is well known that an ideal system can be achieved through overlapping a focal plane, which is usually a Petzval surface, with an image sensor in order to reduce the fundamental aberration. Recently, a curved image sensor was developed [1,2], and this has resulted in a new step being added to optical system design. The advantages, such as the reduced number of optical elements and small package sizes, that result from the curved image sensor have been applied to diverse imaging systems [3–7]. Furthermore, a commercial version of the curved image sensor has already been considered [8]. These sensors have typically been used to design bio-inspired optical systems because there optical devices can provide special features. As a result, research on this topic has been increasing, particularly that mimicking human eyes and insect eyes [1,2,9–11].

However, to date, there has been relatively little research on the ability of these sensors to simplify optical systems. In particular, an imaging system with a wide viewing angle, which is referred to as fisheye camera, has a complex lens configuration comprised of 6–10 lenses (Fig. 1(a)). Although the name of this camera is taken from the visual characteristics of fish eyes, the eye of a fish is composed of only one spherical lens and a curved retina, as depicted in Fig. 1(b) [12]. To date, various fisheye lens systems have been reported and they mimic the wide field of view (FOV) property itself, not the configuration, because realizing a curved image sensor has been almost impossible technically. Now that the research and development of curved image sensors has matured, the simple lens configuration should be considered because it can replace the conventionally complicated optical systems using curvilinear image sensors.

In this paper, a simple fish eye lens system with high performance is reported that utilizes the curved image sensor while exceeding the hemispherical field of view. In this process, three optical systems were designed and evaluated the bioinspired lens structure based on a real fish eye (Fig. 1(c)), hypergon lens-based system (Fig. 1(d)) and Hill sky lens-based system (Fig. 1(e)) previously proposed for wide FOVs [13]. For an optical system inspired by fish eyes (System 1), it is difficult to form a dome-like hemispherical image sensor, and an impractical off-axis brightness characteristic is observed through optical analyses. However, other optical systems such as the hypergon lens system (System 2) and the Hill sky lens-based system (System 3) also exhibit fundamental defects regarding illumination and resolution. Therefore, the proposed system was enhanced through replacing one of the two lenses with a doublet lens (System 4) as illustrated in Fig. 1(f). Through iteratively tailoring the simple fish eye system, the need to reconsider previously proposed optical systems is emphasized because the curved image sensors can offer strategies for old optical systems as simple and high-performance imaging system. Furthermore, in some cases, the combination of natural structures and

* Corresponding author.
E-mail address: ymsong@gist.ac.kr (Y.M. Song).

http://dx.doi.org/10.1016/j.optlastec.2017.04.026
0030-3992/

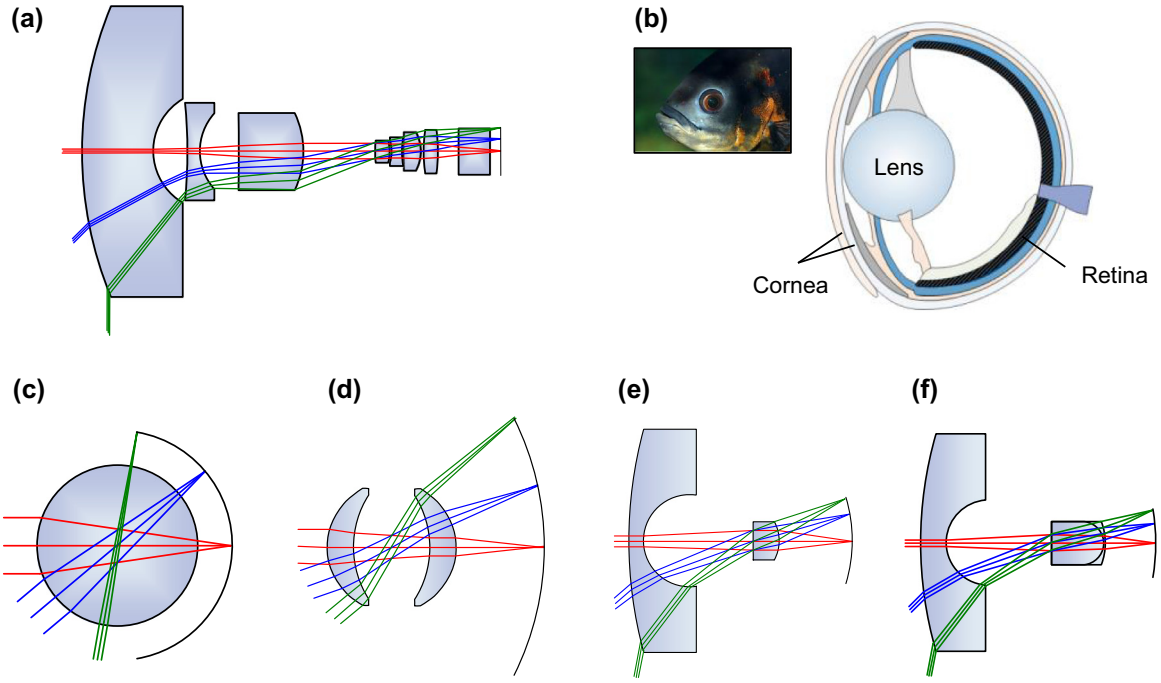

Fig. 1. (a) Conventional fisheye lens optic design with flat image surface [14]. (b) Anatomical image of a teleost eye, which is a representative fish eye in 96% of fish [15]. Inset: image of Astronotus ocellatus [16]. (c) Bio-inspired fisheye lens system (System 1), (d) symmetric optical system (System 2), (e) asymmetric optical system (System 3) with a curved image surface, and (f) Improved asymmetric optical system using a doublet lens (System 4).

artificial design factors (e.g. curved retina and manmade lens configurations) could be more practical and applicable than complete imitation of nature. Details of the design strategies and analysis of the proposed systems are also presented.

2. Simulation methods and optical system design

In order to analyze the lens systems, a sequential ray tracing commercial tool (Zemax, USA) was used to conduct a number of simulations, e.g. spot radius, relative illumination (RI), point spread function (PSF), modulation transfer function (MTF), chromatic focal shift, lateral color, and field curvature. In order to design the proposed optical systems, appropriately constrained merit functions were applied to the overall design process [17].

All optic designs were composed of spherical lens elements only, and a BK7 lens was selected as the base lens. The optical systems were designed in two steps. First, the parameters of the imaging optics, e.g. thickness, lens radii, and distances between each lens, were determined using the local optimization function in the commercial software for wavelengths of 450, 550, and 650 nm. Second, the base lens material (i.e. BK7) was changed to a suitable replacement solution from the library of commercial tool; the parameters were concurrently optimized in order to improve the optical performance using the global optimization function in the software. The information of optimized lens components, such as radii, thicknesses and lens materials for the whole optical systems were listed up in Appendix A.

3. Results and discussion

In order to investigate the resolution characteristics according to the image sensor shapes, i.e. the curved and planar shapes, the spot radius was calculated for each system using the root mean square method as a function of the focus position. The calculated spot radius size for each image sensor type is expressed as a ratio: a_{flat}/a_{curve}, where a_{flat} and a_{curve} are the radius of the spot size on the image plane for the flat and curved image sensors, respectively, for each lens configuration. In order to clearly demonstrate the performance difference depending on the image sensor shape, the values of a_{flat}/a_{curve} were inserted on the focal point (i.e. Focus = 0) with different incident angles as illustrated in Fig. 2(a)–(c). For more accurate comparisons, the radius of curvature (ROC) of the image plane and the F-number of all optical systems were unified to 50 mm and 4, respectively. The ratio of the spot radius means that the larger the ratio of the spot radius, the greater the resolution difference between the planar image sensor and the curved image sensor.

From this perspective, System 1 using a ball lens exhibited the greatest performance improvement when using a curved image sensor compared with the other optical systems because the ratio was more than 1000 at an incident angle of 80°. The size of the spot radius tended to decrease as the incident angle increased, but it is due to the increment of astigmatism, not the resolution grow, as depicted in the inset corresponding to the incident angle of 80° in Fig. 2(a). For the flat image sensor, the spot radius size exponentially increased as the angle increased and became huge with a spot size of approximately 21 mm at an incident angle of 80°. For System 2, the ratio of a_{flat}/a_{curve} increased at a lower rate than System 1. In this system, the astigmatism was more significant at an incident angle of 40° as seen in the inset of Fig. 2(b). Moreover, the illumination converged to 0 due to vignetting at an incident angle of approximately 60°, which can be observed in Fig. 2(d). Therefore, System 2 is not suitable for application in wide FOV imaging systems with curved image sensors. For System 3, the increase in the ratio of a_{flat}/a_{curve} was the smallest among all designs: the performance difference between the flat image sensor and the curved image sensor was not as large as System 1 or System 2. However, in System 3, the increase in astigmatism remained the smallest as the incidence angle increased, as depicted in the inset of Fig. 2(c). These results demonstrate that the curved image sensor provided better optical performance than the flat image sensor in all systems.

Illumination is another critical factor in optical systems; the relative illumination (RI) of each system is compared here. As seen in

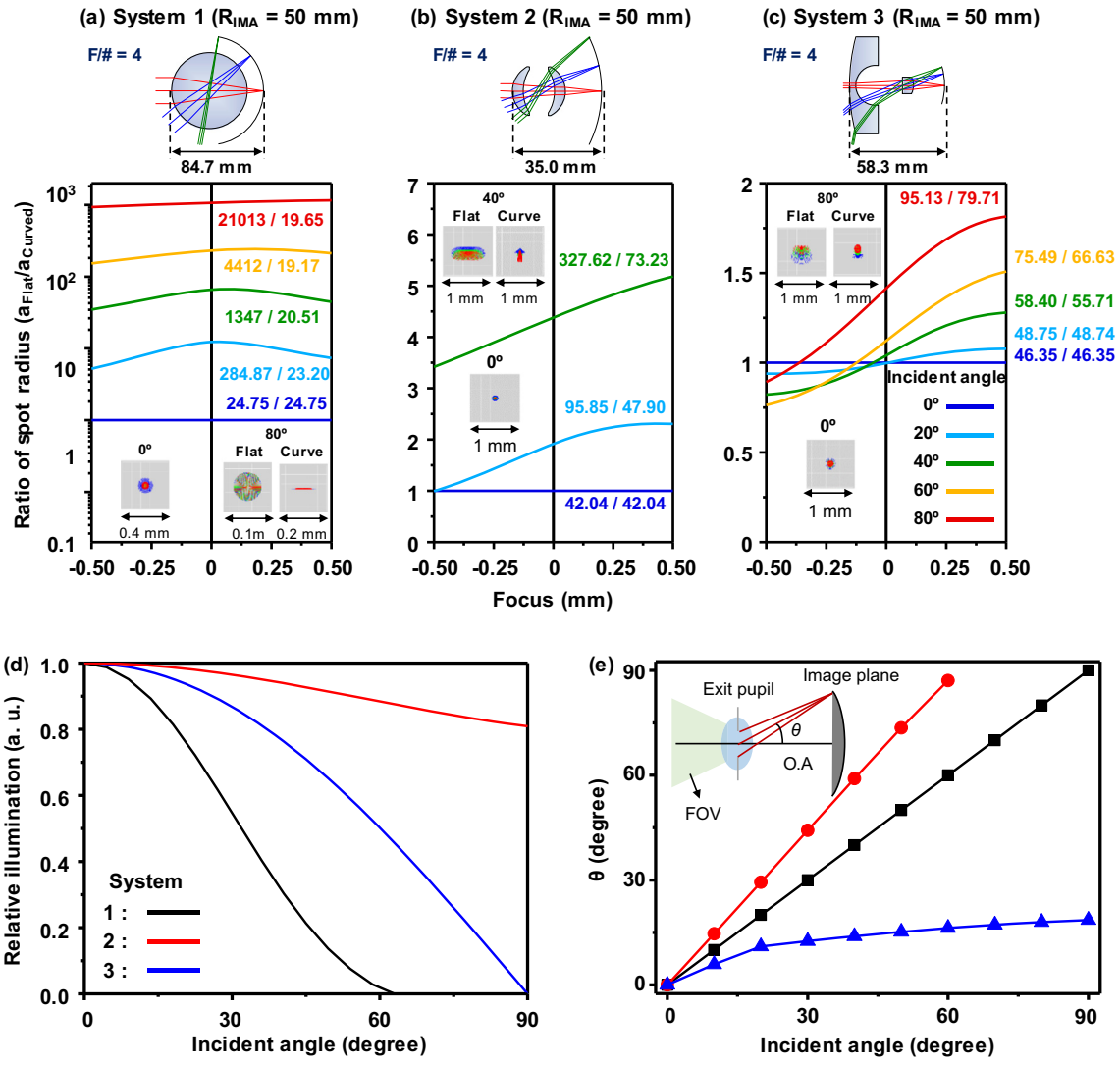

Fig. 2. Ratio of the spot radii for the flat image plane and curved image sensor (ROC = 50 mm) with the same lens configuration, which is illustrated at the top: (a) System 1, (b) System 2, and (c) System 3. All numbers in the graphs are in μm and the spot sizes are at Focus = 0. The insets indicate the distribution of the light beam for wavelengths of 450, 550, and 650 nm as indicated by the blue, green, and red dots, respectively. (d) Relative illumination according to the incident angle at a wavelength of 550 nm for each system. (e) Angle θ as a function of the incident angle at a wavelength of 550 nm for each system. The inset presents a schematic of the definition of angle θ, which is the angle between the ray from an off-axis focal point to the center of the exit pupil and the optical axis. (For interpretation of the references to colour in this figure legend, the reader is referred to the web version of this article.)

Fig. 2(d), the RI was calculated as a function of the incidence angle at a wavelength of 550 nm. This result demonstrates that System 1 and System 2 are inadequate for use in imaging systems with wide FOVs above 120° because their RIs at the off-axis decreased significantly as the incidence angle increased, whereas System 3 is viable for wide FOV imaging systems. This important difference between each system can be explained using the $\cos^4\theta$ dependence of RI, where θ is the angle between the ray from an off-axis focal point to the center of the exit pupil and the optical axis (inset in Fig. 2(e)) [3,18]. However, an exception is the illumination intensity of the ball lens (System 1), which is described as a $\cos\theta$ dependence because all other cosine factors are eliminated due to its geometrical properties [3]. The oblique incident light induced the existence of θ and this increased as the FOV widened; therefore, the optical system should maintain a certain low angle of θ for consistency in the high illumination intensity at the off-axis. In general, for commercial fisheye lens cameras, a minimum of 0.7 RI is required in order to adequately perform the wide FOV property [19]. From this perspective, the optical systems for wide FOVs should be designed to refract the light toward the optical axis beyond the exit pupil in order to enhance the illumination at a full range of angles resembling System 3. Therefore, System 3 is regarded as the most suitable optical system with respect to a wide FOV; however, the resolution should be improved as discussed above.

By replacing one of two lenses in System 3 with a doublet lens, System 4 was designed to enhance the resolution with a ROC of the image surface of 50 mm, which corresponds to that in System 3. The material data for the double lens is also shown in the Table A4 in Appendix A. System 3 and System 4 were compared and evaluated via optical analyses with an F-number of 4. First, MTF simulations were performed for each system at a wavelength of 550 nm as a function of the incident angle. Fig. 3(a) presents the MTFs for both systems. In System 3, the sharpness that can be distinguished is too low (approximately 0 at 10 cycles/mm) and it is difficult to accurately capture the object. The top of Fig. 3(b) shows the PSF of System 3 and illustrate that the PSF was severely spread by the incident angle. In contrast, as illustrated in Fig. 3(a), System 4 exhibited a near diffraction limit straight line, i.e. the black line in the MTF, at a spatial frequency of 10 cycles/mm and had an MTF value of 0.5 or more, except at an incident angle of 100°, up to a

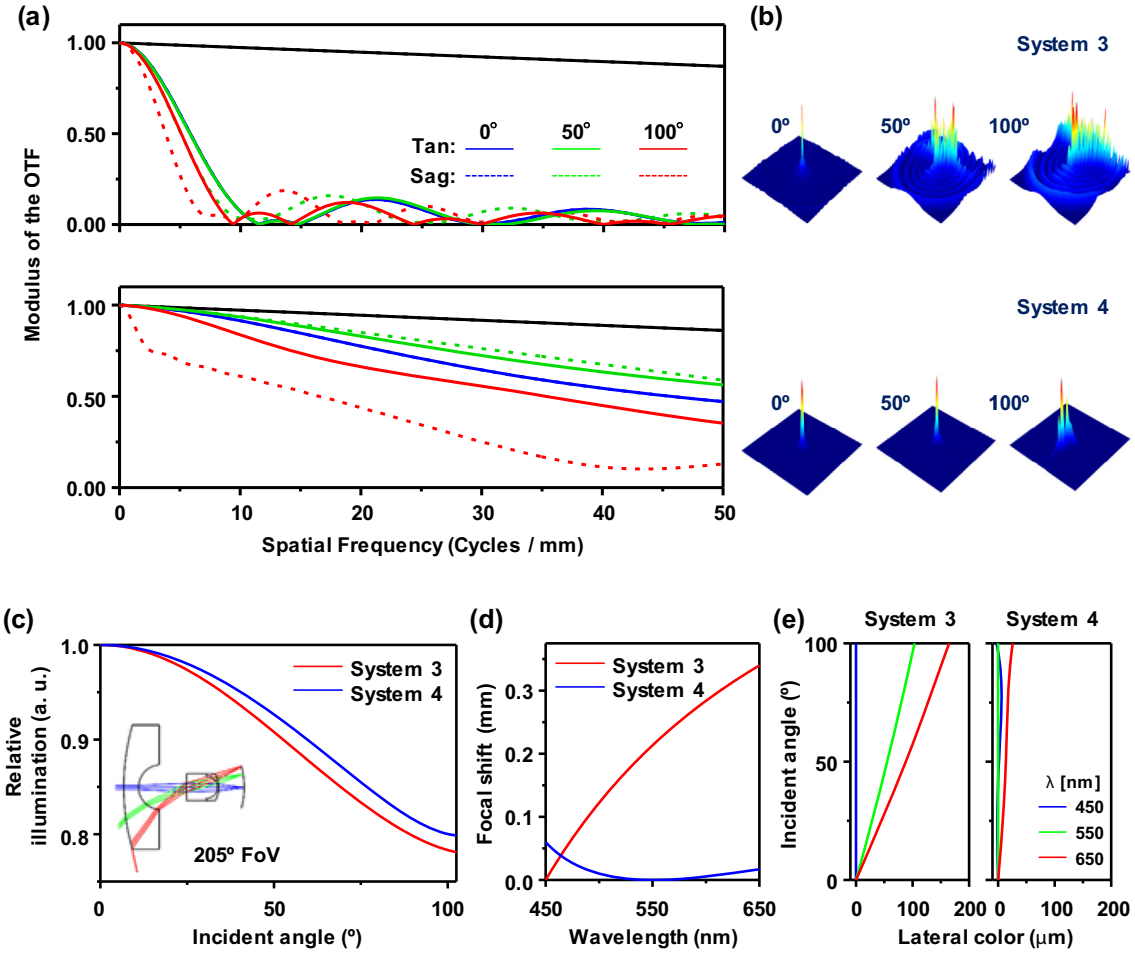

Fig. 3. (a) Modulation transfer functions (MTFs) of System 3 and System 4 for incident angles of 0°, 50°, and 100° at a wavelength of 550 nm. The black lines indicate the diffraction limit of each optical system. (b) The point spreading functions (PSFs) for System 3 and System 4 at a wavelength of 550 nm with different incident angles such as 0°, 50° and 100°. The width and height of the PSFs were 100 μm. (c) Relative illumination for System 3 and System 4 at a wavelength of 550 nm as a function of the incidence angle. The inset depicts the ray-tracing and FOV representation of System 4. (d) Simulated focal shift for each system as a function of the wavelength at a normal incidence. (e) The calculated lateral color spectra versus incidence angle for systems. (d) and (e) present the characteristics related to the chromatic aberration of each system.

spatial frequency of 50 cycles/mm. From a PSF perspective, there is a similar tendency. Almost the same resolution was maintained from 0 to 50°; furthermore, the resolution was good at the incident angle of 100°. Because our proposal optic design has a viewing angle of more than hemispherical FOV (i.e. a hyper FOV), it is suitable for panoramic photography and can be applied in various applications.

To evaluate the availability of our design as the hyper FOV imaging device, the RI was simulated according to the incident angle for each system. Fig. 3(c) presents the illumination characteristics of each system. The results demonstrate that the RI of System 4 is slightly higher than that of System 3 and that the tendencies of both systems are almost equivalent. Both System 3 and System 4 possess FOVs greater than 100°. According to Fig. 2(c), the degree of light refraction by the lens arrangement in System 3 is well suited to obtaining panoramic views. In this respect, System 4 is structurally similar to System 3 and can thus have hyper FOV characteristics. Interestingly, the structure that completely imitates the fish eye (i.e. System 1) cannot have FOV more than 180° because the light above that angle is blocked by the dome-shape image sensor even if the brightness characteristics are maintained. In this respect, a combination of biomimetic and artificial structures can be a more practical solution according to the applications.

Further calculations of the focal shifts as a function of the wavelength, which indicate the longitudinal chromatic aberration and lateral color, were conducted in order to investigate the chromatic aberration of both systems. Fig. 3(d) and (e) compare the chromatic aberration performance of the two systems: both the lateral and the longitudinal chromatic aberrations were significantly improved in System 4. This can be explained by the differences in the dispersion, which resulted from the lenses used in each system, because the doublet lens provided a reduction in the chromatic aberration [20]. In general, for fisheye lens systems, the performance at the edge of an image is as important as the center of the image because two hemispherical images can be digitally stitched together to form a complete 360° image [19]. Therefore, various optical features such as the resolution, RI, and monochromatic and chromatic aberrations should be considered at the wide viewing angle. For these reasons, System 4 can be recommended as the optimum optical system for wide FOVs with high performance and simplicity.

As has been demonstrated, the combination of a curved image sensor and a simple lens configuration has the potential to solve many current drawbacks, such as the large volume, heavy weight, and high cost, in current optical design. However, there is an optimal shape of the image sensor for each lens configuration as we mentioned earlier in Fig. 2(a)–(c). In order to examine the effect of the shape of curved image surfaces, field curvature and PSF simulations were conducted for System 4 with different ROCs for the image surface (ROC_{IMA}). As illustrated in Fig. 4(a), for flat image surfaces, the result had negative values as the incidence angle is increased. This indicates that the focal plane was located in front

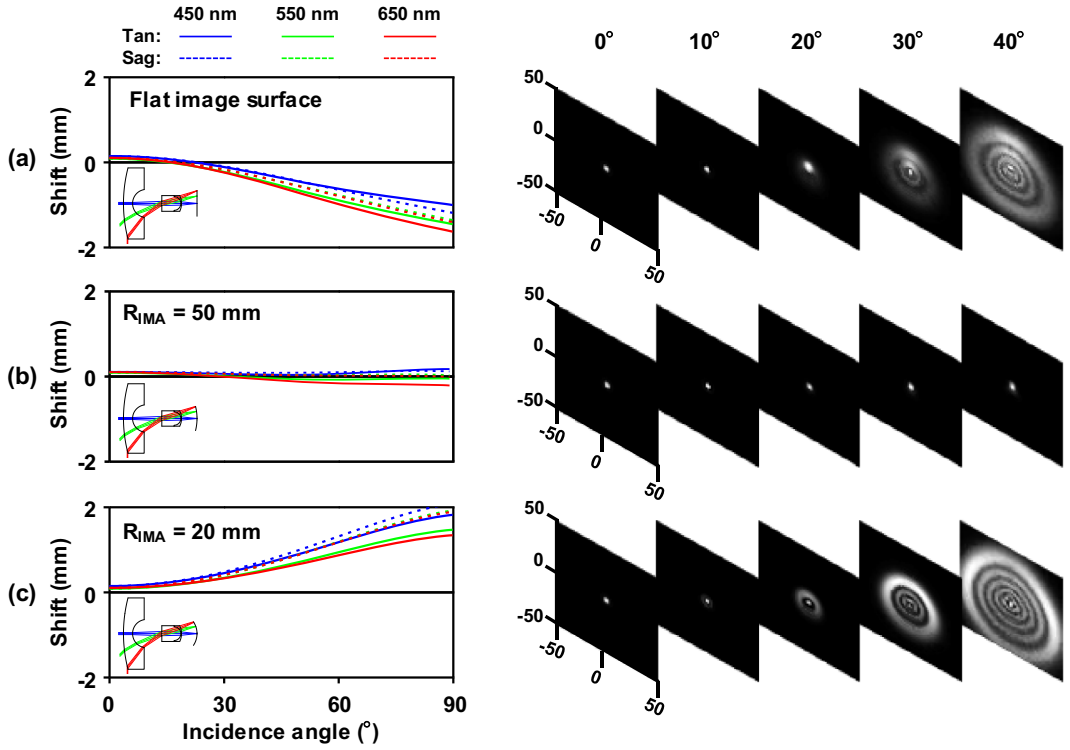

Fig. 4. Simulations of the (left) field curvature and (right) PSF for System 4 with different ROCs: (a) flat image surface (i.e. ROC_{IMA} = infinite), (b) ROC_{IMA} = 50 mm, and (c) ROC_{IMA} = 20 mm. The dimensions along the vertical and horizontal directions in the PSFs are in micrometers.

of the image surface for high incidence angles. This discrepancy induced wider beam spreading as the incident angle increased. The right image in Fig. 4(a) provides useful information for understanding this tendency. In contrast, the field curvature of System 4 with ROC_{IMA} = 50 mm is almost analogous to the black horizontal line as depicted in the left image of Fig. 4(b), and the PSFs of the system continuously exhibit small beam sizes regardless of the incident angle as seen in the right part. This results from the geometrical similarity between the curved image surface and the focal plane. For System 4 with ROC_{IMA} = 20 mm, the focal plane was placed beyond the image surface for oblique incident angles as the field curvatures were positive values as seen in the left of Fig. 4(c). Furthermore, the PSFs were dispersed as the incident angle increased, which is similar to Fig. 4(a), as presented in the right part.

These results demonstrate that a subtle modification of the ROC of the image surface can result in a significant degradation in the image quality. It also indicates that the optimum ROC of the curved image sensor should be considered in designing optical systems in order to match the focal plane. In some cases, an aspheric image sensor such as a parabola or an elliptical sensor may be the optimal structure [4–5].

Fig. 5 presents the results of an image simulation for the object in the inset using the proposed optical systems and the conventional one, in order to compare their overall optical performances. In the process, the sizes of the systems were adjusted in order to obtain an effective focal length (EFL) of 8 mm and an F-number of 4 was used. The object height was set to correspond to an FOV of 140°. All systems were degraded using large distortion because this is an unavoidable problem for wide FOV imaging systems. However, this distortion can be corrected using an algorithm [21]. Fig. 5(a) presents the image simulation of the conventional fisheye lens system as illustrated in Fig. 1(a). Fig. 5(b) and (c) demonstrate that vignetting is clearly visible in System 1 and System 2 due to the drop in RI at the off-axis, as considered in Fig. 2(d).

In particular, the image edges in System 2 are almost black because its RI is almost zero for the incidence angle range above 60°. As depicted in Fig. 5(d), the image simulation of System 3 has uniform brightness; however, blurred parts are clearly observed overall due to the low resolution. Fig. 5(e) demonstrates that System 4 possesses the most effective characteristics with respect to RI and resolution for a wide FOV imaging system with simplicity. The magnified parts of the images are also presented for clarification. These enlarged pictures distinctly demonstrate that the conventional system and the final proposed optical design (System 4) are similar in image quality, except the distortion feature. Various optical aberrations, e.g. distortion, illumination fall-off at off-axis, and low resolution with chromatic aberration, are also visible in other devices.

In order to demonstrate how the final proposed optical design (System 4) successfully simplifies the complexity of the conventional fisheye systems while capturing a wide FOV and good optical properties, such as RI and lateral color, other commercially available systems were considered for comparative analysis. For a thorough comparison, only conventional fisheye lens systems without aspherical optical elements were selected. A summary of the system information is presented in Table 1. Because the typical focal lengths of fisheye lens systems with the popular 35 mm film format are between 8 mm and 10 mm for circular images, the sizes of each system were normalized with an EFL of 8 mm. Although some samples [22–24] possessed shorter axial lengths, which are more feasible for small packaging, than that of System 4, the impractical performances with respect to RI at full field and lateral color become apparent. For the RI, some devices [14,24–26] exhibited more effective values than System 4; however, three systems [14,25,26] necessitated longer axial lengths and one [24] accompanied a defective lateral color characteristic. However, System 4 is superior to the other devices regarding the number of required optical elements, which demonstrates the non-necessity of multi-lens arrangements. Overall, System 4 is an acceptable wide

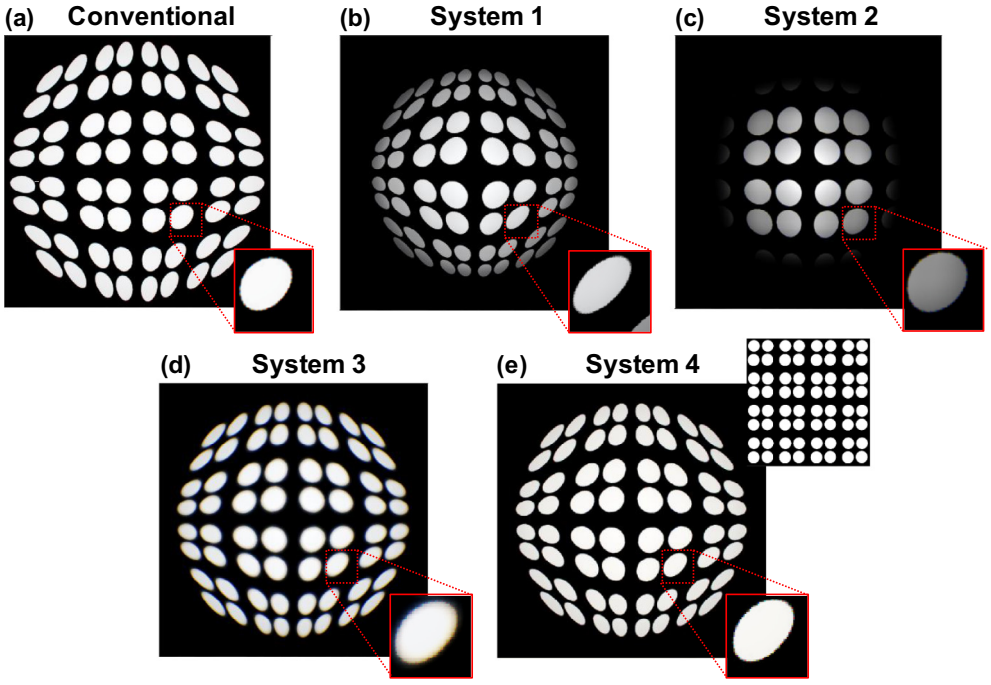

Fig. 5. Image simulations of an object using the proposed optical systems with an effective focal length of 8 mm and an F-number of 4: (a) conventional system, (b) System 1, (c) System 2, (d) System 3, and (e) System 4. The magnified views depict various optical aberrations such as distortion, the illumination fall-off at off-axis, and low resolution with chromatic aberration. The inset is the object used in the simulations.

Table 1
Information of fisheye lens systems.

Number of lens components	Axial length (mm)	FOV (°)	Full field relative illumination (λ = 550 nm)	EFL (mm)	Lateral color at 90° (mm)	Ref.
8	210.94	200	85.8%	8	−0.011	[12]
10	272.24	220	93.6%	8	0.017	[25]
9	50.50	200	57.6%	8	0.013	[22]
10	53.60	190	60.2%	8	0.029	[23]
6	126.17	180	92.5%	8	0.029	[26]
6	57.60	190	82.6%	8	0.131	[24]
3	60.94	205	81.0%	8	0.014	System 4

FOV imaging device with simplicity while reasonably sustaining fundamental optical performances. Moreover, the ability of a curved image sensor to reduce the optical components has a strong potential in the field of light detection/imaging in other spectral ranges, such as infrared (IR) or ultraviolet (UV) light. In those ranges, using fewer lenses are significantly beneficial because optical components for IR and UV are relatively expensive and rare [27–29].

4. Conclusions

In conclusion, four lens structures were designed and analyzed using the advantages of the curved image sensor: a fully bio-inspired fisheye (System 1), a hypergon lens-based system (System 2), a Hill sky lens-based system (System 3), and an advanced Hill sky lens-based system (System 4). These lens configurations demonstrate that the curved image sensor provides better performance than planar image sensors in simple optical systems. In addition, the combination of the curved image sensor and System 4 offers hyper field-of-view (FOV) of over 200° while sustaining a high level of resolution. In this curved image sensor, an optimum radius of curvature (ROC) exists depending on the optical system and a subtle deviation of ROC of curved image sensor from ROC of optimal focal plane occurs serious performance degradation. Moreover, the optical analysis confirmed that the complete bio-inspired structure is not always the best. In some cases, the incorporation of partial biomimetry and artificial design elements yielded better results in practicality and various applications. Furthermore, the curved image sensor is required not only for the wide FOV imaging devices but also for the IR or UV region where the window material is expensive and limited. In this respect, the curvilinear image sensor can be a breakthrough in the development of low cost, simple, small volume, and high resolution imaging systems.

Acknowledgements

This work was supported by Basic Science Research Program of the National Research Foundation of Korea (NRF) (2014R1A1A1005945) and the Korea Basic Science Institute under the R&D program (D37615) supervised by the Ministry of Science, ICT and Future Planning.

Appendix A

See Tables A1–A4.

Table A1
Lens information of System 1 (F-number = 4).

Surface	Radius (mm)	Thickness (mm)	Lens material	Semi-diameter (mm)
Object	Infinity	Infinity		Infinity
1	34.58	34.58	PK50	34.6
Stop	Infinity	0	PK50	5.00
2	Infinity	34.58	PK50	4.10
3	−34.58	15.49		34.60
Image	−50.00	–		49.26

Table A2
Lens information of System 2 (F-number = 4).

Surface	Radius (mm)	Thickness (mm)	Lens material	Semi-diameter (mm)
Object	Infinity	Infinity		Infinity
1	10.81	4.27	N-LAK7	9.59
2	15.9	6.24		8.54
Stop	Infinity	6.24		1.92
3	−15.9	4.27	SSK2	8.54
4	−10.81	13.95		9.6
Image	−50	–		21.11

Table A3
Lens information of System 3 (F-number = 4).

Surface	Radius (mm)	Thickness (mm)	Lens material	Semi-diameter (mm)
Object	Infinity	Infinity		Infinity
1	130.1	8.61	ULTRAN20	40.96
2	13.07	27.46		13.04
Stop	Infinity	0.1		1.93
3	−63	6.55	N-PK51	1.95
4	−6.46	15.56		4.49
Image	−50	–		10.15

Table A4
Lens information of System 4 (F-number = 4).

Surface	Radius (mm)	Thickness (mm)	Lens material	Semi-diameter (mm)
Object	Infinity	Infinity		Infinity
1	135.05	8.93	N-BAK4	37.01
2	13.57	28.5		13.52
Stop	Infinity	0.07		2
3	23.03	18.76	N-LASF31	2.59
4	−6.67	0.67	P-SF68	7.58
5	−17.22	15.2		8.11
Image	−50	–		12.69

References

[1] H.C. Ko, M.P. Stoykovich, J. Song, V. Malyarchuk, W.M. Choi, C.-J. Yu, et al., A hemispherical electronic eye camera based on compressible silicon optoelectronics, Nature 454 (2008) 748–753.
[2] X. Xu, M. Davanco, X. Qi, S.R. Forrest, Direct transfer patterning on three dimensionally deformed surfaces at micrometer resolutions and its application to hemispherical focal plane detector arrays, Org. Electron Phys., Mater. Appl. 9 (2008) 1122–1127.
[3] S.-B. Rim, P.B. Catrysse, R. Dinyari, K. Huang, P. Peumans, The optical advantages of curved focal plane arrays, Opt. Express 16 (2008) 4965–4971.
[4] I. Jung, G. Shin, V. Malyarchuk, J.S. Ha, J.A. Rogers, Paraboloid electronic eye cameras using deformable arrays of photodetectors in hexagonal mesh layouts, Appl. Phys. Lett. 96 (2010).
[5] I. Jung, J. Xiao, V. Malyarchuk, C. Lu, M. Li, Z. Liu, et al., Dynamically tunable hemispherical electronic eye camera system with adjustable zoom capability, Proc. Natl. Acad. Sci. USA 108 (2011) 1788–1793.
[6] D. Dumas, M. Fendler, N. Baier, J. Primot, E. le Coarer, Curved focal plane detector array for wide field cameras, Appl. Opt. 51 (2012) 5419–5424.
[7] D. Dumas, M. Fendler, F. Berger, B. Cloix, C. Pornin, N. Baier, et al., Infrared camera based on a curved retina, Opt. Lett. 37 (2012) 653–655.
[8] R. Sanyal, Sony's curved sensors may allow for simpler lenses and better images, https://www.dpreview.com/articles/2279255612/sony-s-curved-sensors-may-allow-for-simpler-lenses-and-better-images; 2014 [accessed 17.01.06].
[9] K.-H. Jeong, J. Kim, L.P. Lee, Biologically inspired artificial compound eyes, Science 312 (2006) 557–561.
[10] Y.M. Song, Y. Xie, V. Malyarchuk, J. Xiao, I. Jung, K.-J. Choi, et al., Digital cameras with designs inspired by the arthropod eye, Nature 497 (2013) 95–99.
[11] C.C. Huang, X. Wu, H. Liu, B. Aldalali, J.A. Rogers, H. Jiang, Large-field-of-view wide-spectrum artificial reflecting superposition compound eyes, Small 10 (2014) 3050–3057.
[12] R.H.H. Kröger, Optical plasticity in fish lenses, Prog. Retin. Eye Res. 34 (2013) 78–88.
[13] R. Kingslake, A History of the Photographic Lens, 1st ed., Academic Press, Cambridge, 1989.
[14] G.I. Kweon, M. Laikin, Fisheye lens, U.S. patent 8,064,149 B2, 2011.
[15] R.J. Roberts, Fish Pathology, fourth ed., Wiley-Blackwell, New Jersey, 2012.
[16] A. Karwath, Astronotus ocellatus, https://en.wikipedia.org/wiki/Vision_in_fishes; 2006 [accessed 17.01.06].
[17] ZEMAX optical design program user's guide, ZEMAX Development Corporation; 2016.
[18] M. Aggarwal, H. Hua, N. Ahuja, On cosine-fourth and vignetting effects in real lenses, Int. Conf. Comput. Vis. 1 (2001) 472–479.
[19] J.J. Kumler, M.L. Bauer, Fisheye lens designs and their relative performance, Int. Symp. Opt. Sci. Technol. 4093 (2000) 360–369.

[20] A. Miks, J. Novák, P. Novák, Method of zoom lens design, Appl. Opt. 47 (2008) 6088–6098.
[21] T.-Y. Lee, T.-S. Chang, C.-H. Wei, S.-H. Lai, K.-C. Liu, H.-S. Wu, Automatic distortion correction of endoscopic images captured with wide-angle zoom lens, IEEE Trans. Biomed. Eng. 60 (2013) 2603–2613.
[22] O. Toshinobu, Wide-angle lens system with corrected lateral aberration, U.S. patent 3,589,798 A, 1971.
[23] O. Toshinobu, Extreme wide angle lens system, U.S. patent 3,597,049, 1971.
[24] Y. Shimizu, K. Kanagawa, Fisheye lens systems, U.S. patent 3,734,600, 1973.
[25] Y. Shimizu, K. Kanagawa, Wide angle fisheye lens, U.S. patent 3,737,214, 1973.
[26] Nakagawa, Ultra-wide angle photographic lens, U.S. patent 3,741,630 1973.
[27] A. Mahmood, S. Dayeh, D.P. Butler, Z.C. Butler, Micromachined infrared sensor arrays on flexible polyimide, Proc. IEEE (2003) 777–782.
[28] X. Sheng, C. Yu, V. Malyarchuk, Y.H. Lee, S. Kim, T. Kim, et al., Silicon-based visible-blind ultraviolet detection and imaging using down-shifting luminophores, Adv. Opt. Mater. 2 (2014) 314–319.
[29] B.R. Johnson, What's different about ultraviolet and infrared optics?, SPIE Crit Rev. 43 (1992) 61–75.